Predictive Control with Reduced Computational Burden in Cascaded H-Bridge Motor Drives

1st Filippo Gemma
Electrical, Computer and Biomedical Engineering Dept
University of Pavia
Pavia, IT
filippo.gemma01@universitadipavia.it

2nd Giulia Tresca
Electrical, Computer and Biomedical Engineering Dept
University of Pavia
Pavia, IT
giulia.tresca@unipv.it

3rd Andrea Volpini
Electrical, Computer and Biomedical Engineering Dept
University of Pavia
Pavia, IT
andrea.volpini01@universitadipavia.it

4th Behrouz Mohammadzadeh
Electrical, Computer and Biomedical Engineering Dept
University of Pavia
Pavia, IT
behrouz.mohammadzadeh01@universitadipavia.it

5th Pericle Zanchetta
Electrical, Computer and Biomedical Engineering Dept
University of Pavia
Pavia, IT
pericle.zanchetta@unipv.it

***Abstract*—This paper presents a predictive control method for a Permanent Magnet Synchronous Motor (PMSM) driven by a seven-level Cascaded H-Bridge inverter. The control is based on a Tree-Based Model-Free Predictive Control and an online calculation of reduced Look-Up Tables. The Tree-Based approach selects the optimal Voltage Vector, reducing the number of tested vectors. The online LUTs handle the generation of gate signals, ensuring online battery balancing by selecting the appropriate switching state. This method reduces the controller's computational effort, improves torque control, lowers switching losses, and manages the battery State of Charge. Additionally, the proposed control technique eliminates the dependency on a load model by introducing a Model-Free approach, based on a recursive least squares (RLS) algorithm to identify the parameters of an Auto-Regressive with Exogenous input (ARX) model. Simulation results confirm the effectiveness of the proposed control for accurate motor control, reduced switching frequency losses, and SOC management.**

***Index Terms*—Finite-Control-Set, Model-Free-Predictive Control, Computational Burden Reduction, SOC Balancing, Switching Losses Reduction, Permanent Magnet Synchronous Motor, Electric Vehicle.**

I. Introduction

Permanent Magnet Synchronous Motors (PMSMs) have become a key component in modern industrial systems due to their outstanding features, including high efficiency, compact size, and superior dynamic performance [1]. These advantages make them well-suited for applications that demand precise and responsive control, such as robotics, electric vehicles, and high-speed machinery. In many of these applications, the PMSM is powered by a multilevel converter directly interfaced with a battery pack, forming a modular and scalable energy conversion system suited for mobile or off-grid scenarios [2, 3]. As such, the development of advanced control strategies for PMSMs remains a central focus to ensure optimal performance, reliability, and adaptability across a wide range of operating conditions. In this context, multilevel converters have emerged as an effective solution for PMSM drives [4], particularly in medium- and high-power applications, due to their ability to generate output voltages with lower harmonic distortion, reduced voltage stress on power devices, and improved efficiency [5].

Among the conventional approaches, Field-Oriented Control (FOC) has long been established as a standard solution for high-performance motor control. However, FOC relies on linear control principles and is typically implemented with PI regulators, which can limit its effectiveness in scenarios requiring fast transient response or robust performance under parameter variations and nonlinearities [6]. This trade-off between dynamic agility and steady-state precision has motivated ongoing research into alternative control frameworks capable of overcoming these limitations.

To enhance the drive control and reduce power losses, many studies have explored advanced control strategies, with Model Predictive Control (MPC) being one of the most effective [7]. However, applying MPC to multilevel converters may be challenging due to the high number of possible voltage vectors (VVs), which increases the computational effort [8]. Additionally, the presence of redundant gate control signals (GCS) complicates implementation, while battery voltage balancing adds further challenges because of the nonlinear behavior of the batteries. To overcome these challenges, several approaches have been proposed. Cell-by-cell-based MPC methods solve the optimization independently for each H-Bridge module [9]. Hierarchical strategies use a two-stage selection process to reduce the number of candidate GCSs [10]. Other techniques include adaptive VV selection [11], IQOCP decomposition [12], and branch-and-bound algorithms [13].

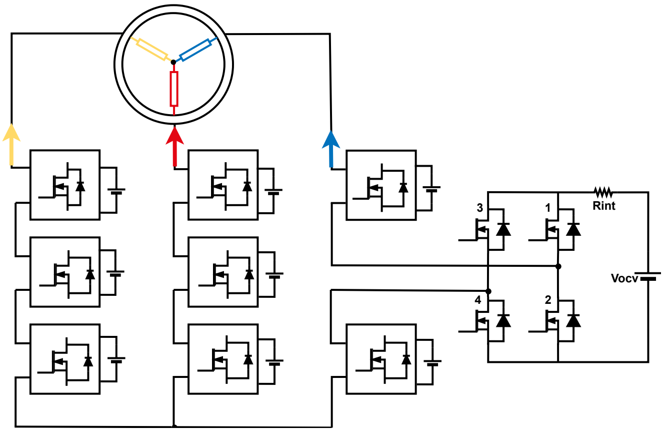

Fig. 1. Cascaded H-Bridge with simplified Li-Ion battery packs and PMSM motor.

A reduced VV selection approach was introduced in [14], limiting the search to adjacent VVs. Offline optimization methods [15] also reduce computation but lack flexibility in real-time scenarios. However, these methods do not consider the battery voltage balancing process.

Therefore, other studies focus mainly on the active battery balancing [16]. Traditional PI and sorting-based methods suffer from low accuracy and reliability [17], [18]. More advanced model-based and rule-based approaches have been proposed [19], [20], along with predictive strategies like variable duty-cycle control [21], nearest-level control [22], and hierarchical distributed control [23]. Only in recent works the MPC is combined with the battery balancing. Dual-stage MPCs enable inter- and intra-arm balancing [24], while single-stage formulations directly optimize submodule active power [25]. Although these approaches may improve performance, they also increase computational cost limiting the real-time applicability [23].

Nevertheless, a critical limitation of MPC is its strong dependence on an accurate system model. Model uncertainties are inevitable due to parameter variations, unmodeled dynamics, and changing environmental conditions. This has led to a growing interest in model-agnostic or adaptive control strategies. Among them, Model-Free Predictive Control (MFPC) has emerged as a promising alternative. Compared to traditional MPC approaches that rely on a fixed global model, MFPC constructs a local model online based on real-time input-output data, thereby enhancing robustness and reducing the need for precise system identification.

Therefore, this paper proposes a novel approach to reduce the computational cost compared to [26] by introducing a Tree-Based (TB) search for optimal voltage vector selection. The proposed method is Model-Free and relies on a Recursive Least Squares (RLS) algorithm to identify the parameters of an Auto-Regressive with Exogenous input (ARX) model [27]. This model is used to predict the motor currents, enabling a flexible prediction strategy that can be applied to any type of motor, without relying on a detailed motor model [28]. The use

TABLE I
PMSM AND LI-ION BATTERY PACK VALUES.

Variable	Symbol	Value	Unit
Stator Res.	R_s	0.47	Ω
Stator Ind.	$L_d = L_q$	4.15	mH
Rated Torque	T_{em}	15	Nm
Rated Speed	ω_m	3000	rpm
Max. Current	I_{max}	20	A
Rated Voltage	V_n	400	V
Pole Pairs	p	3	#
Perm. Flux Link.	ψ_m	0.255	Wb
Bat. capacity	C_n	0.075	Ah
Bat. Nom. Volt.	Vb_n	108.6	V

of the ARX structure allows the controller to adapt to system variations and uncertainties in real time, improving its robustness in practical scenarios. By relying exclusively on input-output data for prediction, the proposed method streamlines the design process and enhances the generality of the control framework. In addition, separating the VVs selection from Gate Signal selection further reduces the computational load. Once the optimal VV is found, only a reduced set of switching states, generated through online LUTs, is evaluated. These states ensure both battery balancing and reduced switching losses.

The proposed method uses two cost functions: the first one, with a Tree-Based approach, selects the best VV to apply at the next step. The second cost function evaluates $GCSs$, aiming to achieve active balancing and reduced switching losses. The switching states considered in the second cost function are selected from LUTs which are updated online based on the batteries' charge levels. By implementing the TB search, the MFPC approach significantly reduces computational complexity, enabling the practical real-time implementation of the ARX-RLS prediction method that would otherwise be computationally prohibitive.

II. System Model

The motor drive system here analyzed includes Li-Ion batteries, a Cascaded H-bridge (CHB) inverter, and a PMSM, as shown in Fig. 1.

A. Modeling of PMSM and Batteries

Key electrical and mechanical specifications for the PMSM and the battery packs are listed in Table I. Each battery pack is modeled using an equivalent circuit composed of an open-circuit voltage (V_{ocv}), which depends on the state of charge (SOC), and an internal resistance (R_{int}) [3]. The open-circuit voltage captures how the terminal voltage varies with SOC, while the internal resistance models losses and voltage drops during operations.

The PMSM is described in the dq rotating reference frame aligned with the rotor flux [29]. The model assumes: 1) linear magnetic behavior and 2) ideal switching of the converter. The dq-axis voltage equations are:

$$\begin{cases} v_d = R_s i_d + L_d \frac{di_d}{dt} - \omega_e i_q L_q \\ v_q = R_s i_q + L_q \frac{di_q}{dt} + \omega_e \left(i_d L_d + \psi_m \right) \end{cases} \tag{1}$$

The electromagnetic torque is expressed as:

$$T_{em} = \frac{3}{2} p \left(i_q \left(i_d L_d + \psi_m \right) - i_d i_q L_q \right) \tag{2}$$

where i_d and i_q are the stator currents along the d- and q-axes, L_d and L_q are the corresponding inductances, ψ_m is the permanent magnet flux linkage, and ω_e is the electrical rotor speed. R_s represents the stator resistance, and p is the number of pole pairs.

B. Cascaded H-Bridge Inverter Model

The CHB converter is made up of several single-phase H-bridge cells connected in series. This structure enables medium-voltage operation and reduced harmonic content at the output [26]. Each H-bridge module is powered by a separate DC source, which corresponds to a dedicated battery pack. The total number of possible switching states for a three-phase CHB converter with N_{mod} H-Bridge is given by:

$$N_{swc} = 2^{N_{mod}} \tag{3}$$

Each H-Bridge can produce discrete voltage levels depending on its switching pattern [26]. The total number of output voltage levels (m) can be calculated as:

$$m = 2H + 1 \tag{4}$$

where H is the number of H-bridge cells per phase leg. The total number of active switches required is:

$$N_{sw} = 6(m - 1) \tag{5}$$

For a system with three cascaded H-bridges per phase (i.e., $N_{mod} = 18$), the number of switching combinations reaches $2^{18} = 262144$. This exponential growth makes real-time optimization very challenging, highlighting the need for efficient control strategies such as predictive control supported by lookup tables (LUTs).

III. Control Strategy

The overall control structure is shown in Fig. 2. A Proportional-Integral (PI) controller regulates the motor speed and generates the reference dq currents.

The predictive control is organized in two main stages. In the first stage, a Tree-Based Model-Free Predictive Control (TB-MFPC) strategy is used to select the optimal voltage vector. The current prediction at instant $k+1$ relies on an Auto-Regressive model with Exogenous input (ARX), whose parameters are continuously updated using a Recursive Least Squares (RLS) algorithm [27]. This Model-Free prediction approach makes the method applicable to different motor types without requiring prior system modeling. After identifying the optimal voltage vector, the second stage determines the corresponding GCS through online Look-Up Tables, simultaneously accounting for battery balancing and minimizing switching losses.

A. Tree-Based Model-Free-Predictive Control

Within the MFPC framework, the PMSM is modeled as a black box, requiring prior estimation of both the model structure and its parameters before performing predictions. Among the various linear model structures employed for dynamic system representation, the Auto-Regressive model with Exogenous input (ARX) is widely utilized due to its computational efficiency and simplicity. The parameters of the ARX model can be effectively identified using established techniques such as Recursive Least Squares (RLS). Furthermore, ARX models demonstrate resilience in the presence of system nonlinearities, thereby enhancing the robustness of the prediction process [30]. Consequently, this study adopts the ARX model as the basis for black-box prediction within the proposed Tree-Based Predictive Control framework. The ARX-based representation defines a transfer function between input and output in the dq stationary reference frame, defined as follows:

$$\hat{i_d}(k) = \frac{B^{dd}(z^{-1})}{A^d(z^{-1})} v_d(k) + \frac{B^{dq}(z^{-1})}{A^d(z^{-1})} v_q(k) \tag{6}$$

$$\hat{i_q}(k) = \frac{B^{qd}(z^{-1})}{A^q(z^{-1})} v_d(k) + \frac{B^{qq}(z^{-1})}{A^q(z^{-1})} v_q(k) \tag{7}$$

where $\hat{i}_d(k)$ and $\hat{i}_q(k)$ represent the estimated PMSM current components, while $v_d(k)$ and $v_q(k)$ denote the CHB output voltages in the dq reference frame. The polynomial coefficients used in the ARX models (6) and (7) are defined as follows:

$$A^i(z^{-1}) = 1 + a_1^i z^{-1} + ... + a_{n_A}^i z^{-n_A} \tag{8}$$

$$B^{ij}(z^{-1}) = 1 + b_1^{ij} z^{-1} + ... + b_{n_B}^{ij} z^{-n_B} \tag{9}$$

In the polynomial terms $B^{ij}(z^{-1})$, the subscript i refers to the axis (d or q) of the estimated current component, while j denotes the axis of the CHB voltage input. Similarly, in the polynomials $A^i(z^{-1})$, the superscript i indicates the axis of the estimated variable. The ARX model structure is defined by the polynomial orders n_A and n_B, which in this work are set to $n_A = 3$ and $n_B = 2$.

The RLS algorithm is used to compute the coefficients (8) and (9) of the ARX model using measurements obtained from the controlled system. The RLS algorithm comprises a set of recursive equations, with the objective at each iteration being to accurately estimate the parameter vector $\hat{\boldsymbol{\theta}}_{\boldsymbol{d,q}}(k)$:

$$\hat{\boldsymbol{\theta}}_{\boldsymbol{d,q}}(k) = \hat{\boldsymbol{\theta}}_{\boldsymbol{d,q}}(k-1) + \mathbf{G}_{d,q}(k)\, e_{d,q}(k) \tag{10}$$

$$\boldsymbol{G}_{\boldsymbol{d,q}}(k) = \frac{\boldsymbol{P}_{\boldsymbol{d,q}}(k-1)\boldsymbol{\varphi}_{\boldsymbol{d,q}}(k)}{\boldsymbol{\varphi}^{\boldsymbol{T}}_{\boldsymbol{d,q}}(k)\boldsymbol{P}_{\boldsymbol{d,q}}(k-1)\boldsymbol{\varphi}_{\boldsymbol{d,q}}(k) + \lambda} \tag{11}$$

$$\boldsymbol{P}_{\boldsymbol{d,q}}(k) = \frac{1}{\lambda}(\boldsymbol{I} - \boldsymbol{G}_{\boldsymbol{d,q}}(k)\boldsymbol{\varphi}^{\boldsymbol{T}}_{\boldsymbol{d,q}}(k))\boldsymbol{P}_{\boldsymbol{d,q}}(k-1) \tag{12}$$

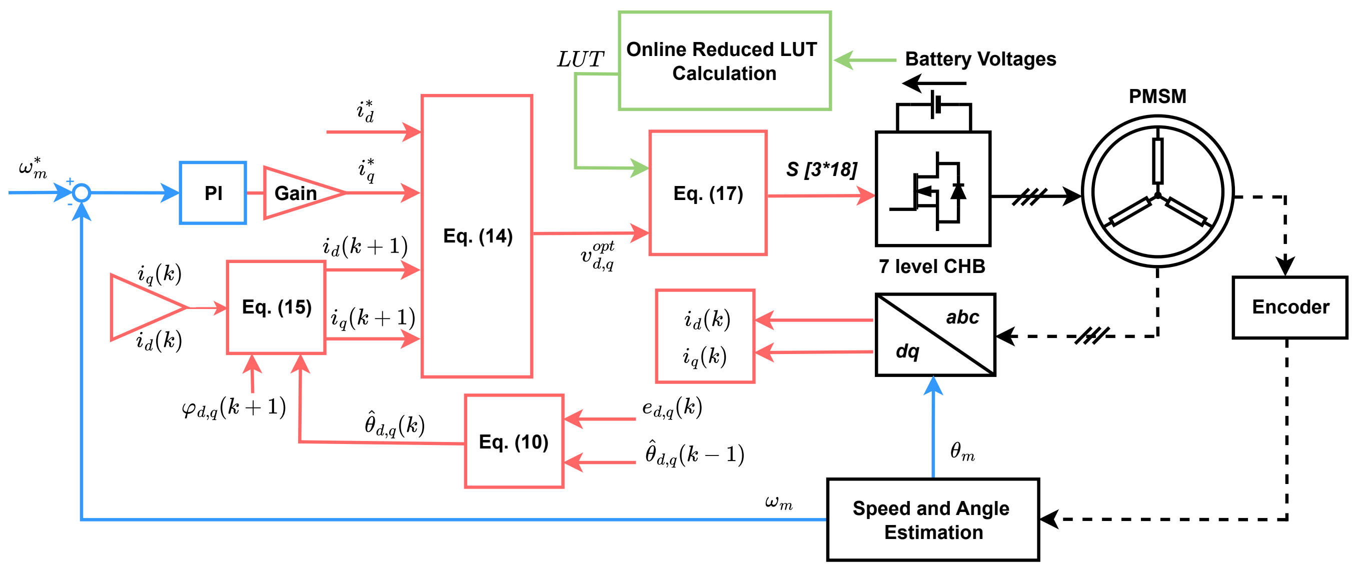

Fig. 2. Proposed control method (f= 20 kHz): (blue) speed control; (red) Torque, balancing and switching losses control; (green) LUT calculation.

The matrix $\boldsymbol{P}_{d,q}(k)$ represents the covariance matrix used in the RLS algorithm. The gain matrix $\boldsymbol{G}_{d,q}\left(k\right)$ links the updated parameters vector at each sampling step with the estimation error $e_{d,q}\left(k\right)$ given by:

$$e_{d,q}\left(k\right) = i_{d,q}(k) - \boldsymbol{\varphi^T_{d,q}}\left(k\right)\boldsymbol{\hat{\theta}_{d,q}}\left(k-1\right) \tag{13}$$

where $i_{d,q}(k)$ are the instantaneous dq current measurements.

The forgetting factor $0 < \lambda \leq 1$ is used in the RLS algorithm to give more importance to recent measurements [27]. Lower values of λ allow the algorithm to quickly follow changes in system parameters, but also increase its sensitivity to noise [31]. In this work, λ is set to 1 to enhance noise rejection, given the high sampling rate of the controller and the assumption that parameter variations occur gradually.

The first cost function for the Tree-Based searching process to determine the v_{dq}^{opt} is:

$$g_1\left(n\right) = \left|\left|\mathbf{i_{d,q}}^* - \mathbf{i_{d,q}}^{k+1}(n) + W_{i_{d,q}}T_s\left(\sum_{j=0}^{m}\mathbf{i_{d,q\,err}}^{k-j}\right)\right|\right|_2^2 \tag{14}$$

The equation (14) evaluates the squared two-norm of the difference between the current references $i^*_{d,q}$ and the current predictions $i^{k+1}_{d,q}(n)$. The current prediction is computed as the scalar product:

$$\mathbf{i_{d,q}}^{k+1}(n) = \boldsymbol{\varphi_{d,q}}^{k+1}\left(n\right)\cdot\boldsymbol{\hat{\theta}_{d,q}}\left(k\right) \tag{15}$$

where $\boldsymbol{\varphi_{d,q}}^{k+1}\left(n\right)$ is defined as:

$$\boldsymbol{\varphi_{d,q}}^{k+1}\left(n\right) = \begin{bmatrix} i_{d,q}(k) \\ i_{d,q}(k-1) \\ i_{d,q}(k-2) \\ v_d(n) \\ v_d(k) \\ v_q(n) \\ v_q(k) \end{bmatrix} \tag{16}$$

The n-index represents the possible voltage vector, while $v_d(n)$ and $v_q(n)$ are the dq voltages generated by the CHB for a n switching combination. T_s is the control sample time (i.e. $T_s = 5e^{-5}$s). The integral term $W_{i_{d,q}}T_s\left(\sum_{j=0}^{m} i_{d,q\,err}^{k-j}\right)$ is used to eliminate the steady-state error [8].

A Tree-Based approach, shown in Fig. 3, is used to find the optimal voltage vector v_{dq}^{opt} to apply to the system. The method relies on a structured, layer-by-layer search strategy. By organizing the search hierarchically, the algorithm limits the number of candidate vectors at each level, reducing computational effort while ensuring good tracking and control performance.

The search starts by evaluating possible candidates in the first layer. The direction that minimizes the cost function in (14) is selected. Then, in the next layer, only the neighboring voltage vectors around the previously chosen one are tested. This process is repeated iteratively until the voltage vector that best approximates the reference is identified.

Following the conclusion of the search, the best candidate $v_{\alpha\beta}^{opt}$ is transformed in v_{dq}^{opt}. Thanks to this hierarchical selection, the number of combinations to evaluate is greatly reduced. For example, a standard MPC for a 7-level CHB would require testing 127 combinations [26]. With the proposed approach, this number drops to a maximum of 22. In

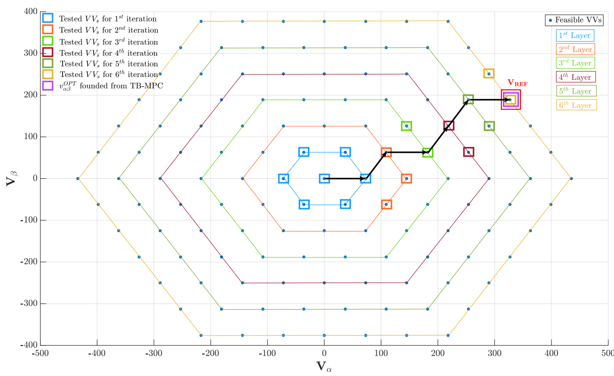

Fig. 3. Tree-Based Model-Free-Predictive Control searching process.

partial-load conditions, even fewer vectors are evaluated. This reduction lowers computational cost and supports fast, real-time control.

B. Online LUTs and Model-Predictive Control

After identifying the optimal voltage vector $v_{d,q}^{opt}$ to apply at time step $k+1$, the second stage of the predictive control selects the most suitable switching state. This choice ensures the application of the selected voltage vector while promoting active battery balancing and reducing switching losses. For a single $v_{d,q}^{opt}$, a set of switching state combinations is retrieved from online Look-Up Tables (LUTs) [26]. These combinations are evaluated using a secondary cost function, defined as follows:

$$g_2(m) = \mu_1 \Delta SOC^{k+1}(m) + \mu_2 \Delta U(m) \tag{17}$$

The first term, $\mu_1 \Delta SOC^{k+1}(m)$, penalizes the differences in the predicted State of Charge (SOC) among battery packs. The SOC at the next step is estimated using the Coulomb counting method [16]:

$$SOC^{k+1}(m) = SOC^k - \frac{T_s \cdot |I_{phase}|}{3600 \cdot C_n} \tag{18}$$

$\Delta SOC^{k+1}(m)$ is the difference between the maximum and minimum predicted SOC values across the battery packs. A large $\Delta SOC^{k+1}(m)$ indicates imbalance and is penalized accordingly.

The second term, $\mu_2 \Delta U(m)$, reduces the switching losses and it is computed as:

$$\Delta U(m) = \frac{n_c(m)}{\text{Total number of switches}} \tag{19}$$

where $n_c(m)$ is the number of switching transitions between time steps k and $k+1$, and the denominator represents the total number of half-bridges in the system. Minimizing this term helps to lower switching frequency and related power losses.

The control command m that minimizes the cost function in (17) is then selected and applied at the next sampling instant.

TABLE II
STATE OF CHARGE STARTING CONDITIONS FOR BATTERY PACK.

	Value	Unit
Phase A	0.90	p.u.
	0.93	p.u.
	0.87	p.u.
Phase B	0.88	p.u.
	0.86	p.u.
	0.95	p.u.
Phase C	0.90	p.u.
	0.91	p.u.
	0.89	p.u.

TABLE III
SIMULATION WEIGHTS.

Weight	$\mu_{1,1}$	$\mu_{1,2}$	$\mu_{1,3}$	$\mu_{2,1}$	$\mu_{2,2}$	$\mu_{2,3}$
Value	30472	300543	0	0.0078	0.00056	0

IV. SIMULATIONS RESULTS

The simulation tests are carried out in MATLAB (Simulink) to validate the effectiveness of the proposed control strategy in regulating both torque and speed of the PMSM, while simultaneously ensuring active balancing of the battery packs. Three representative operating conditions were selected to test the controller: the base speed of the machine ($\omega_b = 3000rpm$), the first field-weakening region ($\omega_{fw} = 4000rpm$), and the second field-weakening region ($\omega_{sw} = 4500rpm$). The initial SOCs values used for the battery modules are reported in Tab. II.

Fig. 4(a) shows the dynamic response of the d and q-current components across the three operating points. The controller ensures accurate tracking of the reference values, even under transients, demonstrating robustness against changes in operating conditions. The corresponding steady-state three-phase currents are depicted in Fig. 4(b), which exhibit acceptable total harmonic distortion (THD). While the average THD is slightly higher than that obtained using classical PI controllers [32], the proposed method guarantees uniform harmonic content across all phases. This is particularly significant given the initial imbalance in battery voltages, as unbalanced phase currents can lead to uneven aging of the electrical machine [33]. This improvement in phase symmetry is attributed to the introduction of a secondary cost function that embeds balancing objectives within the switching state selection process. Mechanical speed tracking is illustrated in Fig. 4(c), confirming that the controller ensures accurate reference tracking during both steady-state and ramp transitions.

Battery voltage evolution under motoring conditions is shown in Fig. 4(d). The proposed control strategy demonstrates its ability to actively balance the pack voltages, despite the initial imbalance both within and across phases. As the machine operates, the voltage discrepancies are progressively reduced. This balancing action is maintained consistently across the different speed ranges, suggesting that the balancing mechanism is effectively decoupled from the torque and speed

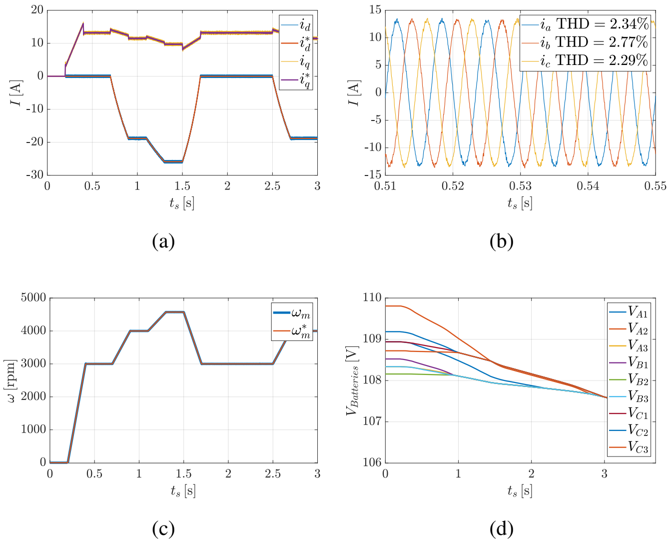

Fig. 4. Simulation results ($\mu_{1,1}$ and $\mu_{2,1}$): (a) i_d and i_q tracking for different operation points; (b) i_{abc} at steady state; (c) ω_m tracking for different operation points; (d) Batteries voltages behavior.

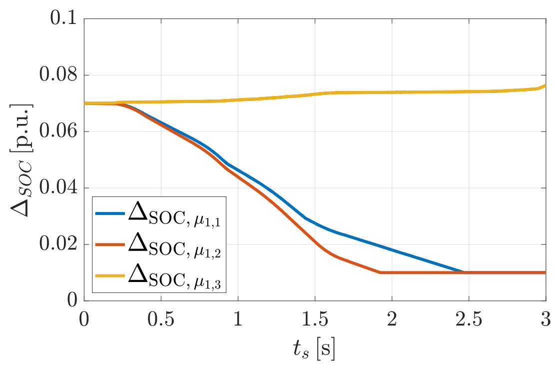

Fig. 5. Batteries SOC behavior during motoring with reference to μ_1 in Tab. III).

regulation tasks.

To evaluate the role of the weighting parameters in the secondary cost function (defined in (17) and listed in Tab. III), the SOC deviation (ΔSOC) and the switching frequency were analyzed under varying values of μ_1 and μ_2, as reported in Fig. 5 and Fig. 6. Increasing μ_1 gives greater priority to balancing, resulting in a faster reduction of SOC deviation. Conversely, decreasing μ_1 slows down the balancing process, which may be beneficial for reducing switching activity. When the secondary cost function is disabled ($\mu_1 = 0$, $\mu_2 = 0$), balancing is no longer achieved and ΔSOC steadily increases, as shown by the yellow curve in Fig. 5.

Similarly, raising the value of μ_2 reduces the switching frequency—see the blue curves in Fig. 6—which contributes to lower switching losses and improved efficiency. However, this also leads to a slower convergence of SOC values. Hence, a trade-off must be established between minimizing

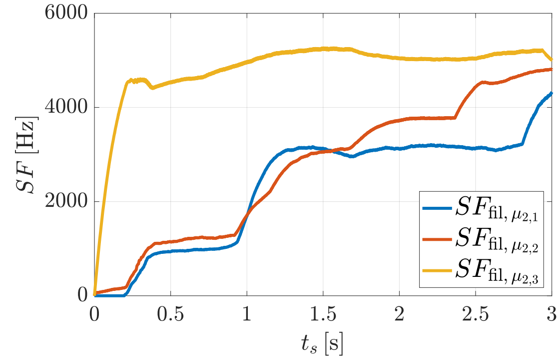

Fig. 6. CHB filtered equivalent switching frequency during motoring with reference to μ_2 in Tab. III.

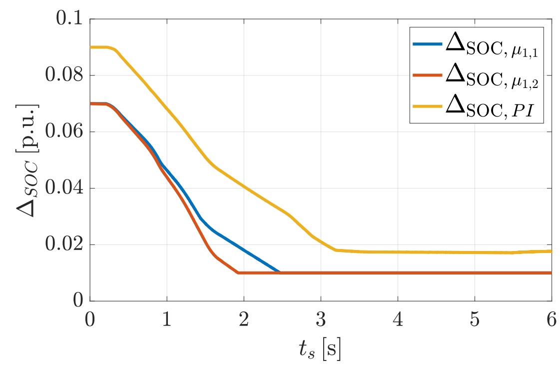

Fig. 7. Batteries SOC behavior during motoring with the proposed control and with the PI.

switching activity and achieving faster balancing. Notably, the integration of the secondary cost function improves both indicators compared to its absence.

A direct performance comparison between the proposed MFPC and a PI-based controller [32] is shown in Fig. 7. The MFPC outperforms the PI-based strategy by achieving faster convergence and lower final SOC deviation, even when balancing is not explicitly prioritized. Furthermore, unlike conventional methods, the proposed strategy does not require the implementation of additional controllers—such as parallel PI loops or duty-cycle modulation techniques—to enforce balancing.

Finally, the dynamic response of the dq current control has been compared with both Model-Based-Predictive controller [26] and conventional PI controller [32]. Fig. 8 demonstrates that the proposed Model-Free strategy exhibits a dynamic response comparable to that of the Model-Based counterpart, despite not relying on explicit machine parameters. When compared with the PI controller (Fig. 9), the proposed approach delivers significantly faster transients and lower overshoot, particularly during simultaneous torque and speed changes. Although the PI controller exhibits slightly reduced steady-state current ripple, the MPFC strategy achieves superior overall performance in terms of responsiveness and balancing.

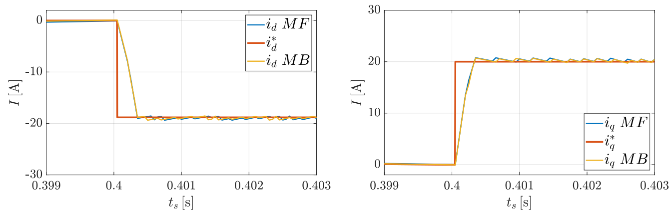

(a) (b)

Fig. 8. Proposed Model-Free versus Model-Based [26], dynamic response to step variation: (a) d-axis; (b) q-axis.

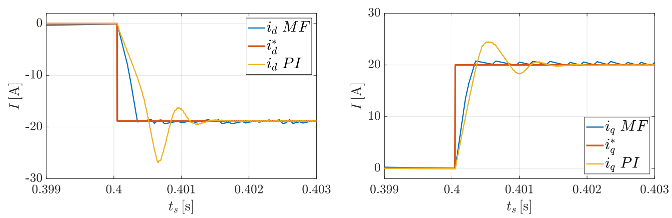

(a) (b)

Fig. 9. Proposed Model-Free versus PI [32], dynamic response to step variation: (a) d-axis; (b) q-axis.

V. Conclusions

This paper presents a Model-Free-Predictive Control (MFPC) strategy for PMSM drives powered by a Cascaded H-Bridge, with integrated active battery balancing. The proposed approach ensures accurate torque and speed regulation across a wide operating range, including field-weakening conditions, while effectively equalizing the State of Charge (SOC) among battery modules. The multi-objective cost function (17) enables a flexible trade-off between switching frequency and balancing speed. Simulation results confirm the robustness and superior performance of the MFPC compared to conventional PI-based and Model-Based controllers, without requiring explicit motor parameters or additional balancing circuits.

VI. Acknowledgment

This work was supported by the Marie Skłodowska-Curie Actions (MSCA) under the European Union's Horizon 2020 Research and Innovation Staff Exchange (RISE) under Grant 872001.

References

[1] J. Yang, J. Chen, W. Liu, G. Yang, and C. Zhang, "Research on torque characteristics of the pmsm with the same number of poles and slots," *IEEE Transactions on Transportation Electrification*, vol. 11, no. 1, pp. 3028–3036, 2025.

[2] G. Tresca, A. Formentini, F. Gemma, F. Lusardi, R. Leuzzi, and P. Zanchetta, "Soc governed algorithm for an ev cascaded h-bridge connected to a dc charger," in *2022 24th European Conference on Power Electronics and Applications (EPE'22 ECCE Europe)*, 2022, pp. 1–9.

[3] F. Gemma, G. Tresca, S. R. Di Salvo, A. Formentini, and P. Zanchetta, "A novel charging approach to temperature and state of charge management in bev," in *2023 IEEE Energy Conversion Congress and Exposition (ECCE)*, 2023, pp. 2706–2712.

[4] D. Ronanki and S. S. Williamson, "Modular multilevel converters for transportation electrification: Challenges and opportunities," *IEEE Transactions on Transportation Electrification*, vol. 4, no. 2, pp. 399–407, 2018.

[5] A. Poorfakhraei, M. Narimani, and A. Emadi, "A review of multilevel inverter topologies in electric vehicles: Current status and future trends," *IEEE Open Journal of Power Electronics*, vol. 2, pp. 155–170, 2021.

[6] Z. Wang, J. Chen, M. Cheng, and K. T. Chau, "Field-oriented control and direct torque control for paralleled vsis fed pmsm drives with variable switching frequencies," *IEEE Transactions on Power Electronics*, vol. 31, no. 3, pp. 2417–2428, 2016.

[7] J. Rodriguez, C. Garcia, A. Mora, F. Flores-Bahamonde, P. Acuna, M. Novak, Y. Zhang, L. Tarisciotti, S. A. Davari, Z. Zhang, F. Wang, M. Norambuena, T. Dragicevic, F. Blaabjerg, T. Geyer, R. Kennel, D. A. Khaburi, M. Abdelrahem, Z. Zhang, N. Mijatovic, and R. P. Aguilera, "Latest advances of model predictive control in electrical drives—part i: Basic concepts and advanced strategies," *IEEE Transactions on Power Electronics*, vol. 37, no. 4, pp. 3927–3942, 2022.

[8] F. Gemma, J. Riccio, G. Tresca, O. Benfatto, and P. Zanchetta, "Finite-control-set model-predictive control of open-end winding synchronous reluctance motor drives," in *2025 IEEE Workshop on Electrical Machines Design, Control and Diagnosis (WEMDCD)*, 2025, pp. 1–6.

[9] C. Qi, X. Chen, P. Tu, and P. Wang, "Cell-by-cell-based finite-control-set model predictive control for a single-phase cascaded h-bridge rectifier," *IEEE Transactions on Power Electronics*, vol. 33, no. 2, pp. 1654–1665, 2018.

[10] T. He, M. Wu, R. P. Aguilera, D. D.-C. Lu, Q. Liu, and S. Vazquez, "Low computational burden model predictive control for single-phase cascaded h-bridge converters without weighting factor," *IEEE Transactions on Industrial Electronics*, vol. 70, no. 3, pp. 2396–2406, 2023.

[11] P. Karamanakos, K. Pavlou, and S. Manias, "An enumeration-based model predictive control strategy for the cascaded h-bridge multilevel rectifier," *IEEE Transactions on Industrial Electronics*, vol. 61, no. 7, pp. 3480–3489, 2014.

[12] Y. Zhang, X. Wu, X. Yuan, Y. Wang, and P. Dai, "Fast model predictive control for multilevel cascaded h-bridge statcom with polynomial computation time," *IEEE Transactions on Industrial Electronics*, vol. 63, no. 8, pp. 5231–5243, 2016.

[13] Y. Zhang, X. Wu, and X. Yuan, "A simplified branch and bound approach for model predictive control of multi-

level cascaded h-bridge statcom," *IEEE Transactions on Industrial Electronics*, vol. 64, no. 10, pp. 7634–7644, 2017.

[14] Q. Xiao, Y. Jin, H. Jia, Y. Mu, Y. Ji, R. Teodorescu, and F. Blaabjerg, "Modulated model predictive control for multilevel cascaded h-bridge converter-based static synchronous compensator," *IEEE Transactions on Industrial Electronics*, vol. 69, no. 2, pp. 1091–1102, 2022.

[15] G. Scaglione, C. Nevoloso, G. Schettino, A. O. Di Tommaso, and R. Miceli, "A novel multi-objective finite control set model predictive control for ipmsm drive fed by a five-level cascaded h-bridge inverter," *IEEE Journal of Emerging and Selected Topics in Power Electronics*, pp. 1–1, 2024.

[16] F. Gemma, G. Tresca, A. Formentini, and P. Zanchetta, "Balanced charging algorithm for chb in an ev powertrain," *Energies*, vol. 16, no. 14, 2023. [Online]. Available: https://www.mdpi.com/1996-1073/16/14/5565

[17] L. Maharjan, S. Inoue, H. Akagi, and J. Asakura, "State-of-charge (soc)-balancing control of a battery energy storage system based on a cascade pwm converter," *IEEE Transactions on Power Electronics*, vol. 24, no. 6, pp. 1628–1636, 2009.

[18] F. Gao, L. Zhang, Q. Zhou, M. Chen, T. Xu, and S. Hu, "State-of-charge balancing control strategy of battery energy storage system based on modular multilevel converter," in *2014 IEEE Energy Conversion Congress and Exposition (ECCE)*, 2014, pp. 2567–2574.

[19] E. Chatzinikolaou and D. J. Rogers, "Cell soc balancing using a cascaded full-bridge multilevel converter in battery energy storage systems," *IEEE Transactions on Industrial Electronics*, vol. 63, no. 9, pp. 5394–5402, 2016.

[20] H. Xue, J. He, Y. Ren, and P. Guo, "Seamless fault-tolerant control for cascaded h-bridge converters based battery energy storage system," *IEEE Transactions on Industrial Electronics*, vol. 70, no. 4, pp. 3803–3813, 2023.

[21] H. Yao, Y. Yan, Y. Cao, P. Song, and T. Shi, "A variable duty cycle-based predictive control for pmsm fed by cascaded h-bridge inverter," *IEEE Journal of Emerging and Selected Topics in Power Electronics*, vol. 10, no. 4, pp. 4195–4206, 2022.

[22] L. Mathe, P. Dan Burlacu, E. Schaltz, and R. Teodorescu, "Battery pack state of charge balancing algorithm for cascaded h-bridge multilevel converters," pp. 1–6, 2016.

[23] B. Xu, H. Tu, Y. Du, H. Yu, H. Liang, and S. Lukic, "A distributed control architecture for cascaded h-bridge converter with integrated battery energy storage," *IEEE Transactions on Industry Applications*, vol. 57, no. 1, pp. 845–856, 2021.

[24] P. Poblete, R. H. Cuzmar, R. P. Aguilera, J. Pereda, A. M. Alcaide, D. Lu, Y. P. Siwakoti, and G. Konstantinou, "Dual-stage mpc for soc balancing in second-life battery energy storage systems based on delta-connected cascaded h-bridge converters," *IEEE Transactions on Power Electronics*, vol. 40, no. 1, pp. 500–515, 2025.

[25] G. Liang, E. Rodriguez, G. G. Farivar, E. Nunes, G. Konstantinou, C. D. Townsend, R. Leyva, and J. Pou, "Model predictive control for intersubmodule state-of-charge balancing in cascaded h-bridge converter-based battery energy storage systems," *IEEE Transactions on Industrial Electronics*, vol. 71, no. 6, pp. 5777–5786, 2024.

[26] F. Gemma, J. Riccio, G. Tresca, A. Volpini, and P. Zanchetta, "Finite-control-set model predictive control with reduced computational burden in cascaded h-bridge permanent magnet synchronous motor drives for ev applications," in *2024 IEEE Energy Conversion Congress and Exposition (ECCE)*, 2024, pp. 3941–3947.

[27] J. Rodríguez, R. Heydari, Z. Rafiee, H. A. Young, F. Flores-Bahamonde, and M. Shahparasti, "Model-free predictive current control of a voltage source inverter," *IEEE Access*, vol. 8, pp. 211 104–211 114, 2020.

[28] J. Riccio, F. Gemma, L. Rovere, G. Tresca, M. D. Nardo, S. Odhano, M. Degano, and P. Zanchetta, "Effects of the floating capacitor voltage on the torque-speed characteristic of an open-end winding synchronous reluctance motor drive," *IEEE Transactions on Industry Applications*, vol. 61, no. 2, pp. 3269–3278, 2025.

[29] E. Zerdali and P. Wheeler, "Model-free simplified predictive current control of pmsm drive with ultra-local model-based ekf," in *2021 3rd Global Power, Energy and Communication Conference (GPECOM)*, 2021, pp. 62–66.

[30] F. Tinazzi, P. G. Carlet, S. Bolognani, and M. Zigliotto, "Motor parameter-free predictive current control of synchronous motors by recursive least-square self-commissioning model," *IEEE Transactions on Industrial Electronics*, vol. 67, no. 11, pp. 9093–9100, 2020.

[31] D. Park, B. Jun, and J. Kim, "Fast tracking rls algorithm using novel variable forgetting factor with unity zone," *Electronics Letters*, vol. 27, pp. 2150–2151, 1991. [Online]. Available: https://digital-library.theiet.org/doi/abs/10.1049/el%3A19911331

[32] M. Quraan, T. Yeo, and P. Tricoli, "Design and control of modular multilevel converters for battery electric vehicles," *IEEE Transactions on Power Electronics*, vol. 31, no. 1, pp. 507–517, 2016.

[33] A. Bonnett and G. Soukup, "Cause and analysis of stator and rotor failures in three-phase squirrel-cage induction motors," *IEEE Transactions on Industry Applications*, vol. 28, no. 4, pp. 921–937, 1992.